Ferromagnetism, superconductivity and quantum criticality in uranium intermetallics

Nguyen Thanh, H.

Publication date
2008

4. A ferromagnetic quantum critical point in URhGe doped with Ru

4.1. Introduction

In the past decade, URhGe has attracted significant attention because ferromagnetism (Curie temperature T_C = 9.5 K) and unconventional superconductivity (T_S = 0.25 K) coexist at ambient pressure [36]. The superconducting state is believed to have its origin in the proximity to a ferromagnetic instability: near the quantum critical point (QCP), which can be reached by tuning T_C to 0 K, enhanced ferromagnetic spin fluctuations mediate Cooper pairing (of the spin-triplet type [41]). The important role of critical magnetic fluctuations in URhGe is furthermore indicated by field-induced superconductivity for a magnetic field B directed along the orthorhombic b-axis [38]. It has been suggested that the high-field superconducting phase is due to magnetic fluctuations associated with the spin reorientation process, which takes place at $B \approx 12$ T [38]. Clearly, it is of considerable interest to further investigate the magnetic properties of URhGe, especially in view of the proximity to a magnetic instability.

The crystallographic, magnetic, transport and thermal properties of URhGe have been investigated in much detail on polycrystalline as well as on single crystalline samples [39,113-120]. URhGe crystallizes in the orthorhombic TiNiSi structure (space group *Pnma*) [39]. Itinerant ferromagnetic order is found below T_C = 9.5 K [39] and the ordered moment of about 0.4 μ_B/U-atom points along the orthorhombic c-axis [36,119]. The linear electronic coefficient in the specific heat γ = 0.16 J/molK^2 is enhanced, which indicates that URhGe is a correlated metal [115].

The application of hydrostatic [120] or uniaxial pressure [121] drives URhGe away from the magnetic instability as the Curie temperature increases. This opens up the possibility to search for a magnetic instability in URhGe by negative chemical pressure. A draw-back is that superconductivity will be suppressed because of the induced disorder.

According to literature, among the neighboring TiNiSi isostructural U*T*Ge compounds (*T* = transition metal), only URuGe and UCoGe† have a paramagnetic ground state [39,40], see Fig. 4.1. Notice that the compound URhSi is also isostructural to URhGe and ferromagnetic with a Curie temperature of 9.5 K [39,115,117]. These observations indicate doping with Ru or Co could possibly lead to a reduction of T_C and the approach to the magnetic instability.

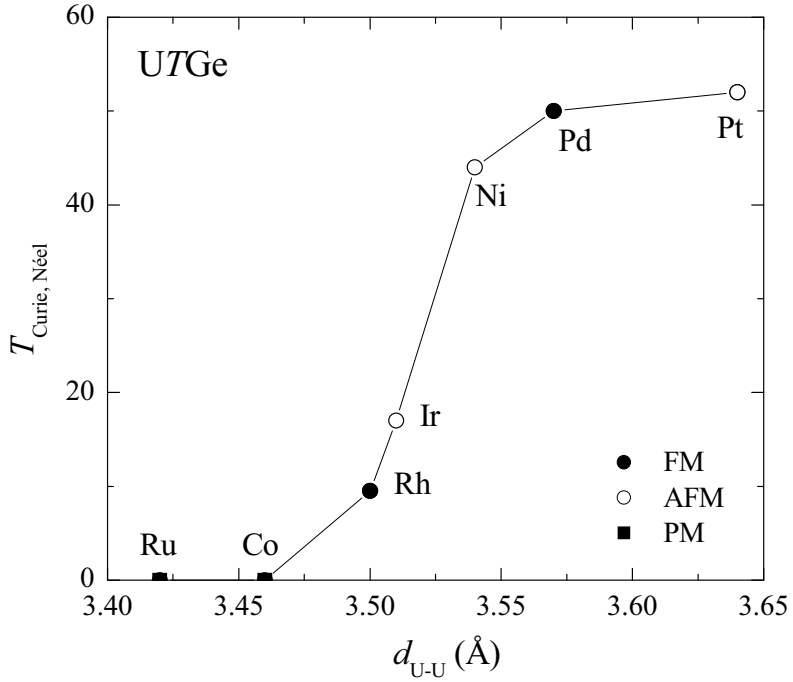

Figure 4.1 The magnetic ordering temperature, T_{Curie} (●) or $T_{Néel}$ (○), of U*T*Ge compounds (*T* = transition metal) as a function of the shortest Uranium - Uranium distance, d_{U-U}. URhGe is located on near the non-magnetic - magnetic borderline. The data are taken from Ref.[40]. The solid line is a guide to the eye. All compounds adopt the TiNiSi structure except UPdGe with crystallizes in the orthorhombic $CeCu_2$ structure [39].

In this chapter, we report our investigations of the magnetic, transport and thermal properties of polycrystalline samples of the $URh_{1-x}Ru_xGe$ series. The main result is that ferromagnetism is suppressed upon Ru doping and vanishes at the critical concentration

† In the course of this work we have discovered that UCoGe orders ferromagnetically at 3 K (see Chapters 6&7)

x_{cr} = 0.38. The observed non-Fermi Liquid (NFL) T dependencies of the specific heat and electrical resistivity, together with the smooth suppression of the ordered moment, provide evidence for a continuous FM Quantum Phase Transition (QPT). This classifies $URh_{1-x}Ru_xGe$ as one of the scarce f-electron systems in which a FM QCP at ambient pressure can be reached by doping.

A study of the evolution of ferromagnetism in URhGe doped with Si and Co will be reported in Chapter 6.

4.2. Sample preparation and characterization

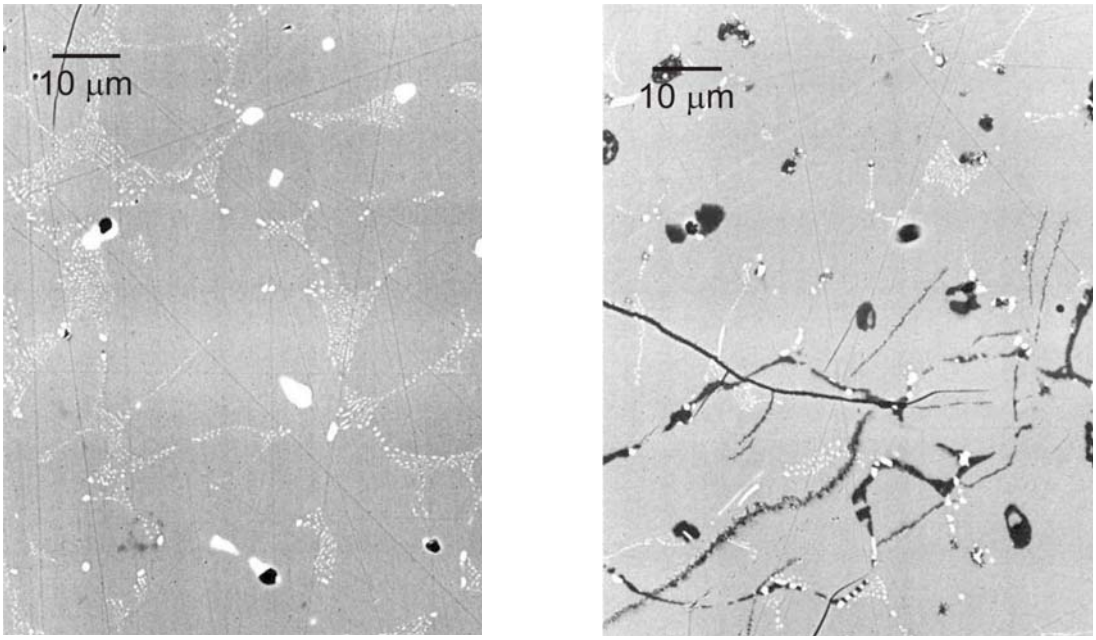

Figure 4.2 EPMA micrographs of URhGe (*left panel*) and $URh_{0.8}Ru_{0.2}Ge$ (*right panel*). The grey areas represent the main matrix. The (big and small) light spots are the Uranium rich phases. The black spots and black lines are holes and cracks on the surface, respectively.

A series of polycrystalline $URh_{1-x}Ru_xGe$ samples with x in the range $0 \leq x \leq 1$ were prepared from nominal compositions $U_{1.02}$(Rh,Ru)Ge by arc-melting the constituents U, Rh, Ru (all 3N purity) and Ge (5N purity) under a high-purity argon atmosphere. Here an excess of 2% U was added to compensate for the Uranium loss during arc melting because of its high vapor pressure. The weight loss of the samples after arc melting was less than 0.1%. The as-cast buttons were annealed for 10 days at 875 ^{o}C. The samples were then cut by spark erosion in bar- and cube-shapes for the different experiments.

The phase homogeneity of the annealed samples was investigated by electron micro-probe

analysis (EPMA) on different positions on the samples. For all compounds, the main matrix forms about 98% of the samples. A small amount (2 - 3%) of Uranium rich impurity phases is detected mainly located at the grain boundaries (see Fig. 4.2). The EPMA pictures show tiny cracks on the micro-scale in the samples in which Rh is replaced by Ru. Composition analysis was carried out with the Wavelength Dispersive X-ray Spectroscopy (WDS) technique. Because of the similar atomic numbers, the main energy spectra of Rh and Ru almost overlap which hampers the determination of the atomic ratio between Rh and Ru. Therefore, the compositions of our samples are defined as nominal compositions.

X-ray powder diffraction confirmed the orthorhombic TiNiSi structure (space group *Pnma*) [119,122] for all samples in the $URh_{1-x}Ru_xGe$ series. The lattice parameters have been determined for the samples with $x \leq 0.60$ (data taken by S. Sakarya [123]). The results are shown in Fig. 4.3 together with literature data for pure URuGe [39]. For URhGe the values $a = 6.887$ Å, $b = 4.334$ Å and $c = 7.513$ Å are in good agreement with literature values (the uncertainty in the determination of the lattice parameters is about 0.1 %). The variation of

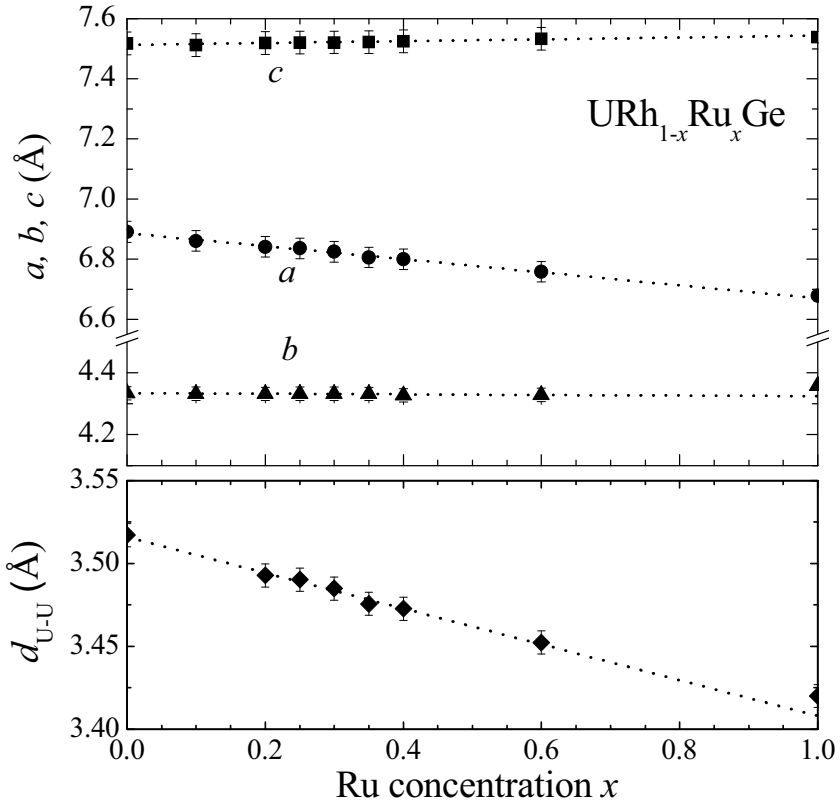

Figure 4.3 Upper frame: Lattice parameters of $URh_{1-x}Ru_xGe$ as a function of the Ru concentration x measured at room temperature. *Lower frame*: The shortest Uranium-Uranium distance of $URh_{1-x}Ru_xGe$ as a function of the Ru concentration x. Data for URuGe are taken from Ref.[39].

the lattice parameters upon doping is anisotropic. The *a* lattice parameter shows the largest variation, it reduces linearly with increasing *x*. The *c* parameter shows a small increase, while the *b* parameter remains almost constant. The unit cell volume Ω = 224.2 Å^3 for URhGe follows Vegard's law [124] and decreases linearly at a rate of 0.067 Å^3/at.% Ru. The extrapolated value of Ω for URuGe amounts to 217.5 Å^3, which is slightly smaller than the literature value of 219.5 Å^3 [39]. This difference is mainly due to the smaller extrapolated value for the *b* lattice parameter compared to the literature value (see Fig. 4.3).

The shortest Uranium-Uranium distance, $d_{U\text{-}U}$, calculated from the structural parameters is shown in the lower frame of Fig. 4.3. For URhGe the value of $d_{U\text{-}U}$ is equal to of 3.51 Å which compares well with the Hill limit of 3.4 - 3.6 Å [125]. $d_{U\text{-}U}$ linearly decreases upon Ru doping with a slope of -1.1×10^{-3} Å/at.% Ru. This provides evidence for itinerant electron states in $URh_{1-x}Ru_xGe$ alloys.

4.3. Magnetic properties

The temperature variation of the magnetization, $M(T)$, of the $URh_{1-x}Ru_xGe$ series measured in a field of 0.01 T is shown in Fig. 4.4. Also shown, in the lower part of the figure, is the derivative $dM(T)/dT$. The inflection point in $M(T)$ or the temperature at which $dM(T)/dT$ has a minimum defines the Curie temperature T_C. For pure URhGe the Curie temperature T_C is 9.6 K, in good agreement with previous values reported in the literature [36,39,115]. Upon replacing Rh by Ru the ferromagnetic transition first shifts upwards to 10.6 K for x = 0.05. For higher concentrations, the magnetic order is suppressed in a monotonic way. At x = 0.15, T_C attains the same value as for pure URhGe and beyond x = 0.20 T_C decreases approximately linearly with x at a rate of -0.43 K/at.% Ru. For the samples with x > 0.35, no magnetic transition was observed in the dc-magnetization (measured for T > 1.8 K).

For a ferromagnet, the general expression for the temperature-dependent magnetization $M(T)$ for $T < T_C$ is given by:

$$M(T) = M_0(1-(T/T_C)^{\alpha})^{\beta} \qquad (4.1)$$

where M_0 is the magnetization extrapolated to T = 0, α is a phenomenological parameter which reflects the ferromagnetic spin-wave contribution at low temperature $T \ll T_C$, and β is the temperature critical exponent of the magnetization near T_C. Notice that the magnetization is measured in a small field B = 0.01 T, at which the moment is not

saturated yet. The M_0 value therefore can be smaller than the spontaneous moment M_S. For pure URhGe, $M(T)$ is well fitted with $M_0 = 0.11\ \mu_B$/f.u., $\alpha = 2$ and $\beta = 0.29$ (the fit is not shown in Fig. 4.4). Here α deviates from the usual spin-wave exponent $\alpha = 3/2$ [126]. For the Ru-doped compounds the analysis becomes more difficult due to an energy gap which opens in the magnon spectrum (see the analysis of the specific-heat data in Section 4.5). Nevertheless, focusing on the behavior near T_C, we extract a critical exponent $\beta = 0.3$ - 0.4 for $x \leq 0.25$ when fixing the spin-wave exponent $\alpha = 2$. The β values obtained in this way are close to the theoretical value $\beta = 0.325$ predicted for 3D Ising-like magnets [127,128].

For all samples in addition the field variation of the magnetization, $M(B)$, was measured up to 5 T at a number of fixed temperatures. By making Arrott plots [129], *i.e.* by plotting the data as M^2 versus $\mu_0 H/M$, T_C is identified by the isotherm that intersects the origin. Typical Arrott plots are presented in Fig. 4.5 for $x = 0$ and 0.325. Ideally, the isotherms should be linear. The upward curvature at higher values of $\mu_0 H/M$ is due to spin

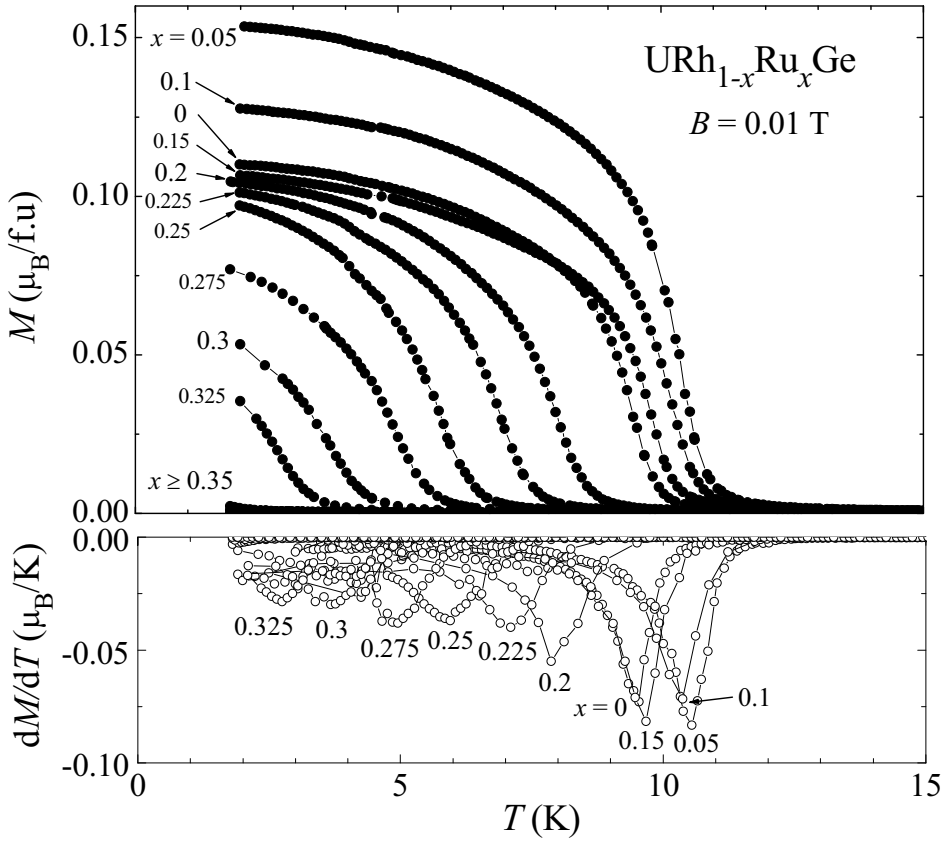

Figure 4.4 Upper frame: Temperature variation of the dc magnetization measured in a field $B = 0.01$ T of $URh_{1-x}Ru_xGe$ alloys. Notice T_C first increases and has a maximum value for $x = 0.05$. For $0.35 \leq x \leq 1$ magnetic order is not observed above $T = 1.8$ K. The solid lines connect the data points. *Lower frame*: Temperature derivative of the magnetization.

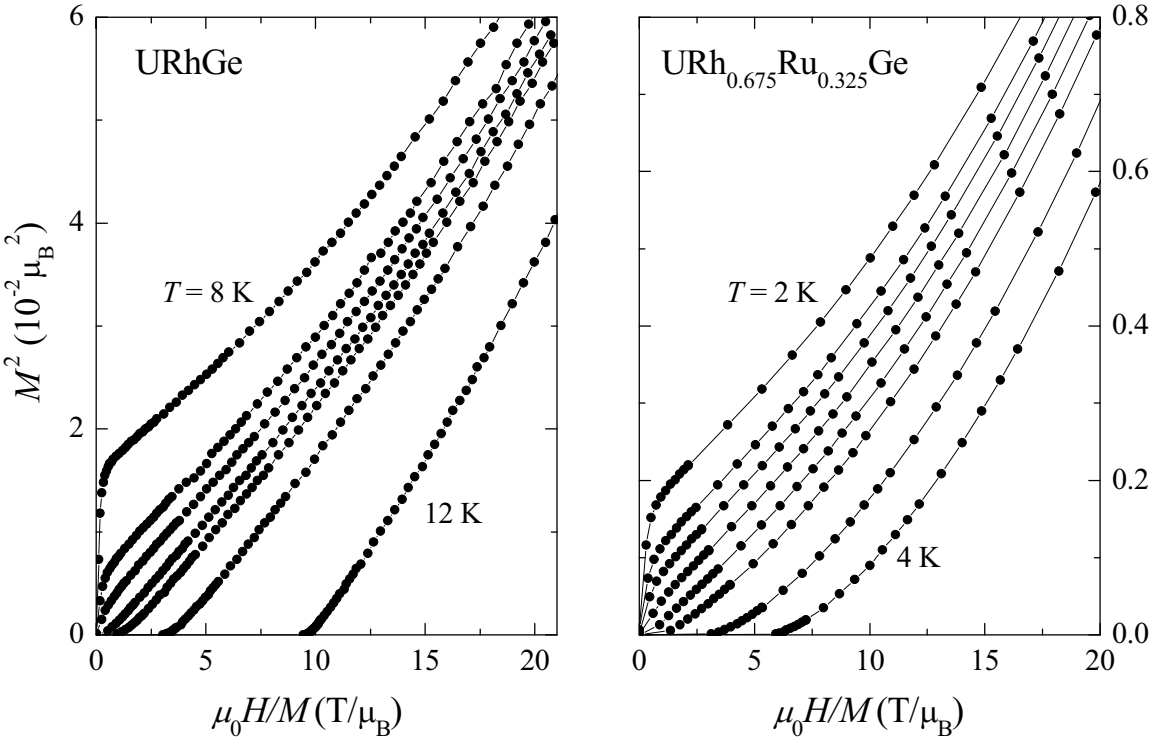

Figure 4.5 Arrott plots of the magnetization of (*left panel*) URhGe with the isotherms measured (from top to down) at T = 8.0, 9.2, 9.5, 9.8, 10.0, 10.5 and 12.0 K and (*right panel*) $URh_{0.675}Ru_{0.325}Ge$ with the isotherms measured (from top to down) at T = 2.0, 2.4, 2.6, 2.8, 3.0, 3.2, 3.6 and 4.0 K. The isotherm through the origin determines T_C = 9.6 and 2.8 K for URhGe and $URh_{0.675}Ru_{0.325}Ge$, respectively.

reorientation processes (from the easy axis to the applied magnetic field) [38] of the magnetic moments in our polycrystalline samples.

The Curie temperatures deduced from the Arrott plots (neglecting the small error in the determination of T_C due to demagnetization effects) T_C = 9.6 and 2.8 K for x = 0 and 0.325, respectively, are in good agreement with those derived from the minimum in d$M(T)$/dT. The Arrott plot of the compound with x = 0.35 (not shown) suggests that ferromagnetism sets in near $T_C \sim 1.3$ K. This value of T_C is estimated by extrapolating the intersection points of the isotherms with the $\mu_0 H/M$ axis to the origin of the Arrott plot. For x = 0.375, T_C is close to zero, while for $x \geq 0.38$ the Arrott plots clearly indicate a paramagnetic ground state. T_C obtained by the magnetization measurements are listed in Table 4.1.

Hysteresis loops of the $URh_{1-x}Ru_xGe$ alloys measured at the temperature a 2 K in magnetic field range -0.3 T $\leq B \leq$ 0.3 T are shown in Fig. 4.6. The symmetric loops corroborate ferromagnetic order with small ordered moments. The reduction of the remnant moment and the size of the coercive field upon Ru doping, display the suppression of

ferromagnetism in the system. For $x > 0.35$, the magnetization linearly depends on the magnetic field with a small slope dM/dH and no hysteresis effects are observed, indicating a paramagnetic state at 2 K. The ordered moment can be extracted by extrapolating $B \rightarrow 0$

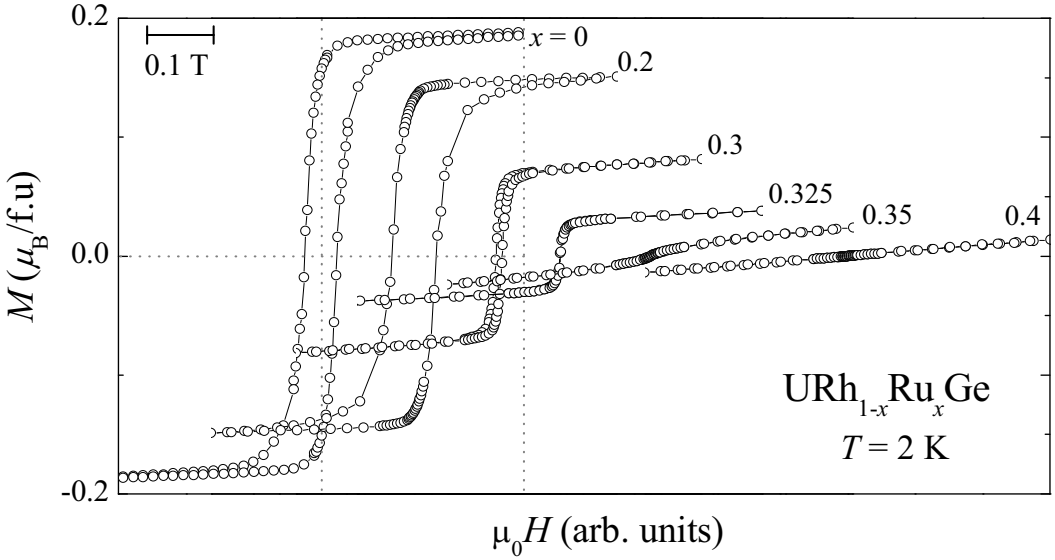

Figure 4.6 Hysteresis loops of $URh_{1-x}Ru_xGe$ alloys measured at the temperature of 2 K. The bar gives an absolute field scale. Ru concentrations are (from left to right) x = 0, 0.2, 0.3, 0.325, 0.35 and 0.4.

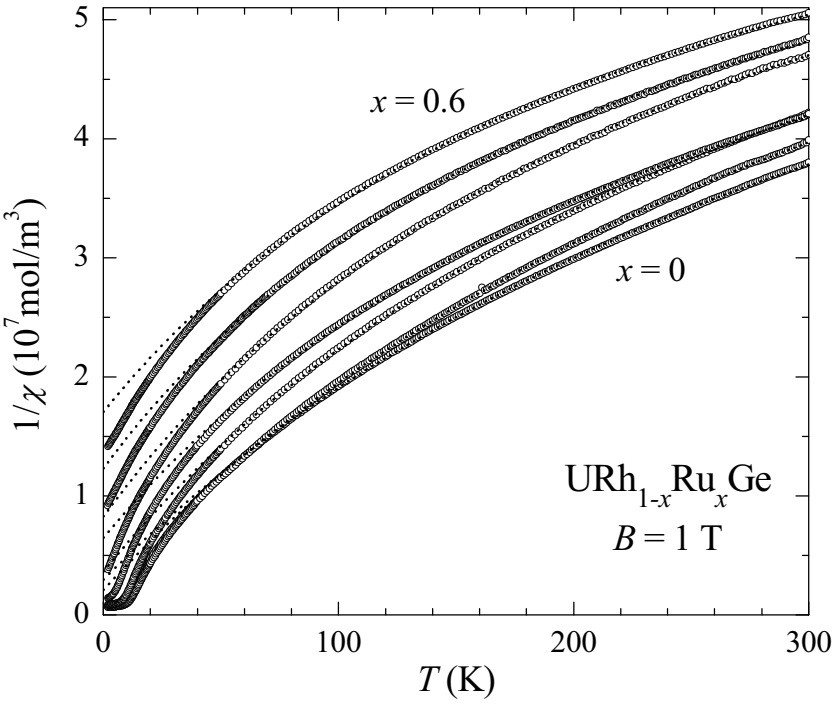

Figure 4.7 Temperature variation of the inverse susceptibility $1/\chi$ of selected $URh_{1-x}Ru_xGe$ alloys measured in a field of 1 T. The dotted lines are the best fits to the MCW law in the temperature range T = 50 - 300 K. Ru concentrations are (from bottom to top) x = 0, 0.1, 0.2, 0.3, 0.4, 0.5 and 0.6.

from field values above the coercive fields, $B \gg B_C$. The values of the ordered moments are 0.18, 0.15, 0.07, 0.05 μ_B/f.u. for x = 0, 0.2, 0.3, 0.325, respectively.

Fig. 4.7 shows the reciprocal susceptibility, $1/\chi$, of a few selected $URh_{1-x}Ru_xGe$ alloys measured in a field B = 1 T in the temperature range 2 - 300 K. In uranium intermetallics the high temperature local-moment susceptibility is usually described by the modified Curie-Weiss (MCW) law:

$$\chi(T) = \chi_0 + \frac{C}{T-\theta} \qquad (4.2)$$

where χ_0 represents a temperature independent contribution. The strong magneto-crystalline anisotropy, observed in single-crystalline URhGe samples [119], hampers, however, the proper analysis of the susceptibility of our polycrystalline samples. The analysis is further complicated by the strong curvature of $1/\chi$ versus T, which probably originates from the random orientation of the magnetocrystalline anisotropy axes in the crystallites with respect to the applied magnetic field. Note that in pure URhGe the easy-axis (c-axis) susceptibility measured on a single crystal does follow a MCW behavior with $\theta \approx T_C$ = 9.5 K, as demonstrated in Ref.[36]. For our polycrystals, the best fits to MCW behavior are obtained in the temperature range 50 - 300 K. These yield a slight decrease of the effective moment p_{eff} from 1.72 to 1.26 μ_B for x = 0 to 0.6, respectively, and a roughly x-dependent χ_0 value of about ~ 10^{-8} m^3/mol. The overall upward shift of the curves with increasing Ru contents indicates an increasing (antiferromagnetic) interaction strength θ. The values of p_{eff} and θ of $URh_{1-x}Ru_xGe$ by fitted $\chi(T)$ to Eq. 4.2 are summaried in Table 4.1.

The field dependence of the magnetization of the $URh_{1-x}Ru_xGe$ series is measured in fields up to 5 and 50 T at 2 and 4.2 K, respectively (see Figs. 4.8 and 4.9). The magnetization curves are well described by an empirical exponential function [130]:

$$M(H) = M_S + \Delta M(1 - e^{-\mu_0 H / B_0}) \qquad (4.3)$$

Here the parameter B_0 probes the magnetic interaction strength of the fluctuating itinerant moments, M_S is the spontaneous magnetization, and ΔM determines the high field moment $M(H = \infty) = M_S + \Delta M$. Extrapolation of M versus B to $B = 0$ yields an estimate of M_S. The M_S values are almost the same for both low- and high-field magnetization fits and coincide with the ordered moment values inferred from the hysteresis loops (see Fig. 4.6). For pure URhGe, $M_S \approx 0.18$ μ_B in agreement with the polycrystalline average ½m_0 for a

uniaxial FM [131] (m_0 = 0.4 μ_B directed along the *c* axis [36]). The spontaneous moment M_S extracted by fitting the experimental data $M(H)$ to Eq. 4.3 of $URh_{1-x}Ru_xGe$ is traced in Fig. 4.10. $M_S(x)$ follows the same trend as T_C versus Ru concentration. The $M_S(x)$ values

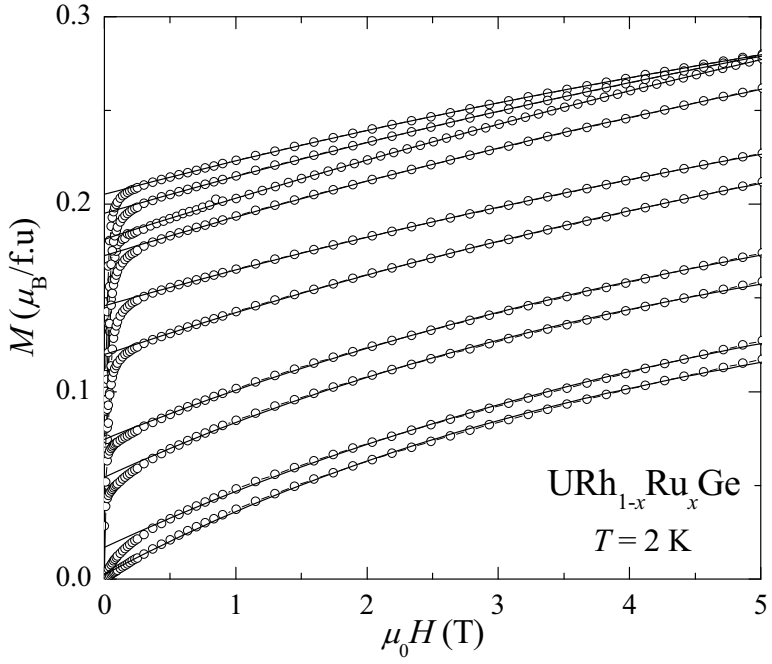

Figure 4.8 Field dependence of the magnetization of $URh_{1-x}Ru_xGe$ alloys measured in a field up to 5 T at 2 K. The solid lines represent fits to Eq. 4.3. Ru concentrations are (from top to bottom) x = 0.05, 0.1, 0, 0.15, 0.2, 0.25, 0.3, 0.325, 0.35 and 0.4.

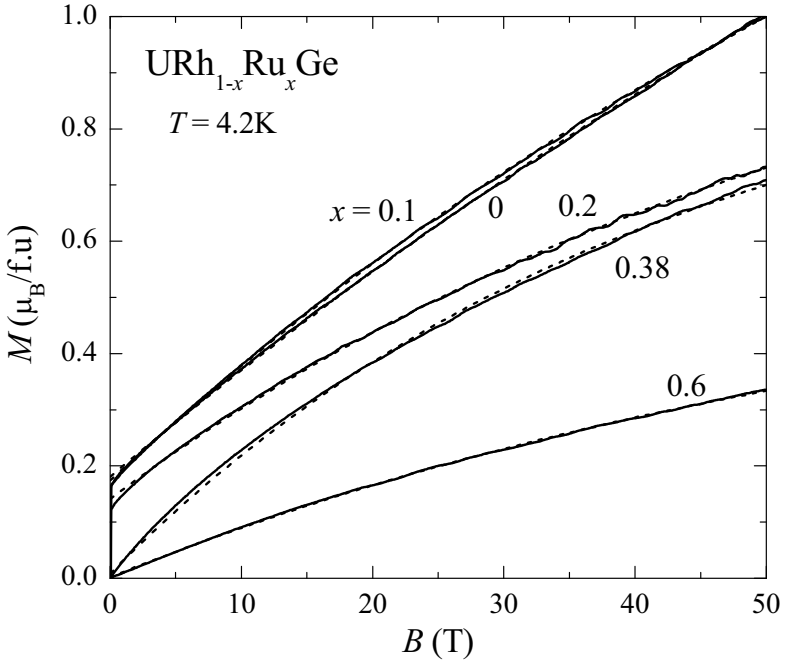

Figure 4.9 High-field magnetization of $URh_{1-x}Ru_xGe$ alloys measured in a field up to 50 T at 4.2 K. The dotted lines indicate fits to Eq. 4.3. Ru concentrations are (from top to bottom) x = 0.1, 0, 0.2, 0.25, 0.38 and 0.6.

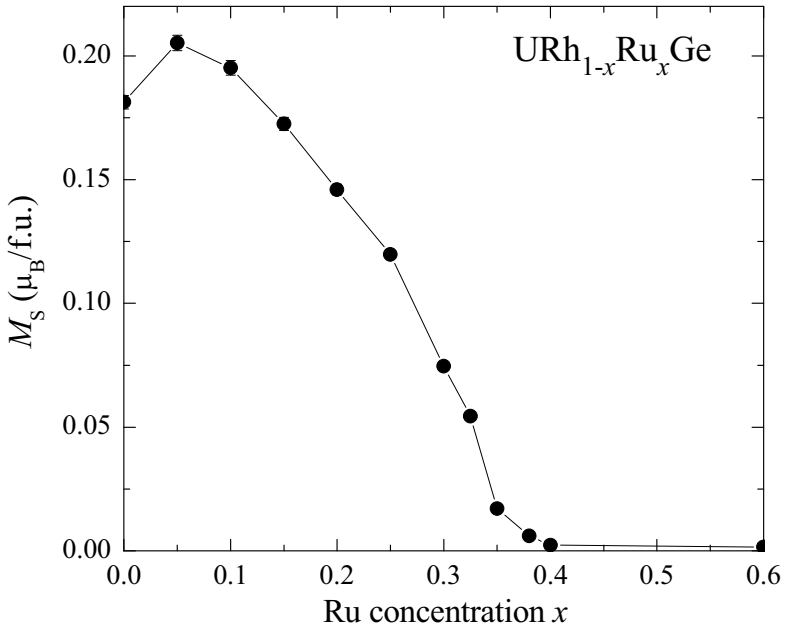

Figure 4.10 The spontaneous moment M_S obtained by fitting $M(H)$ to Eq. 4.3 for $URh_{1-x}Ru_xGe$ as a function of Ru concentration.

reveals a shallow maximum at $x = 0.05$ and smoothly go to 0 at a critical concentration near $x = 0.4$. This shows that the FM to paramagnetic transition as a function of x is a continuous (second order) phase transition.

Itinerant magnetism is characterized by a large ratio of the effective moment p_{eff} to the spontaneous moment M_S [82,132], in marked contrast to localized FM in which $p_{eff}/M_S \sim 1$. The large values of p_{eff}/M_S increasing with Ru concentration confirm predominantly itinerant *f*-electron character in our $URh_{1-x}Ru_xGe$ alloys.

High-field magnetization experiments have been carried out to investigate the evolution of the spin-reorientation process observed in pure URhGe [38] (the uniaxial moment with size of 0.4 μ_B rotates from the *c*-axis to the *b*-axis for a field of 12 T along the *b*-axis) as a function of Ru concentration. However, no sign of such a spin-reorientation process was detected in the ordered state at 4.2 K in magnetic fields up to 50 T. This we attribute to the averaging effect on the uniaxial process in polycrystals and the relatively high measuring temperature. $M(H = \infty)$ extracted from the high-field measurement shows a decrease from the value of 2.84 to 0.60 μ_B/f.u. for $x = 0$ to 0.6. These values are still smaller than the saturation magnetization values for the free ion Uranium $5f^2$ (3.58 μ_B) and $5f^3$ (3.62 μ_B) configuration.

Table 4.1 The Curie temperature T_C, the spontaneous moment M_S, the effective moment p_{eff} and the paramagnetic Curie temperature θ of the $URh_{1-x}Ru_xGe$ alloys deduced from magnetization measurements.

x-Ru	T_C (K)	M_S (μ_B/f.u.)	p_{eff} (μ_B/f.u.)	θ (K)
0	9.6	0.18	1.72	-14.1
0.05	10.6	0.21	1.78	-6.2
0.1	10.4	0.20	1.68	-9.4
0.15	9.7	0.17	1.72	-7.8
0.2	8.1	0.15	1.55	-14.3
0.25	6.0	0.12	1.54	-15.3
0.3	3.7	0.08	1.49	-24.8
0.325	2.8	0.05	1.43	-22.7
0.35	1.3	0.02	1.42	-31.6
0.38	-	0.01	1.42	-26.7
0.4	-	0.00	1.38	-27.5
0.5	-	-	1.30	-39.0
0.6	-	0.00	1.26	-54.2

4.4. Electrical resistivity

The temperature dependence of the electrical resistivity $\rho(T)$ of the $URh_{1-x}Ru_xGe$ alloys is shown in Fig. 4.11. Note that the vertical scale is in arbitrary units and the curves are shifted for clarity.

For $x \leq 0.60$ the overall temperature variation (see the left panel in Fig. 4.11) is consistent with the formation of a Kondo-lattice, *i.e.* an increase of the resistivity upon lowering T below 300 K, a weak broad maximum in the temperature range 110 - 150 K and a steady drop signaling coherence at low temperatures. For all doped samples the absolute variation of the resistivity in the temperature interval 2 - 300 K amounts to 150 - 250 μΩcm, which are usual values for uranium intermetallics [40,114]. The residual resistivity values ρ_0 are large (200 - 500 μΩcm) and do not follow a systematic variation with Ru concentration. This is mainly attributed to the brittleness of the samples. Micro-cracks appear in the Ru-doped samples, as demonstrated by the EPMA micrograph for $x = 0.2$ in the left panel of Fig. 4.2. Consequently, the residual resistance ratio ($RRR = \rho(300\ K)/\rho_0$) for URhGe is 6, and amounts to ~ 2 for the substituted samples.

The right panel in Fig. 4.11 shows $\rho(T)$ in the temperature interval 0.25 - 15 K. For $x = 0$ the kink in $\rho(T)$ signals the Curie temperature, T_C = 9.4 K, in agreement with the magnetization data. Below T_C the resistivity is dominated by spin-wave scattering, while for $T \geq T_C$ spin-disorder scattering is dominant. We did not observe any sign of superconductivity in the URhGe sample for temperatures down to 0.25 K, which we attribute to the low *RRR* = 6 and the corresponding small mean free path [41]. With increasing x the kink at T_C becomes less pronounced. However, for all $x \leq 0.35$, T_C can be

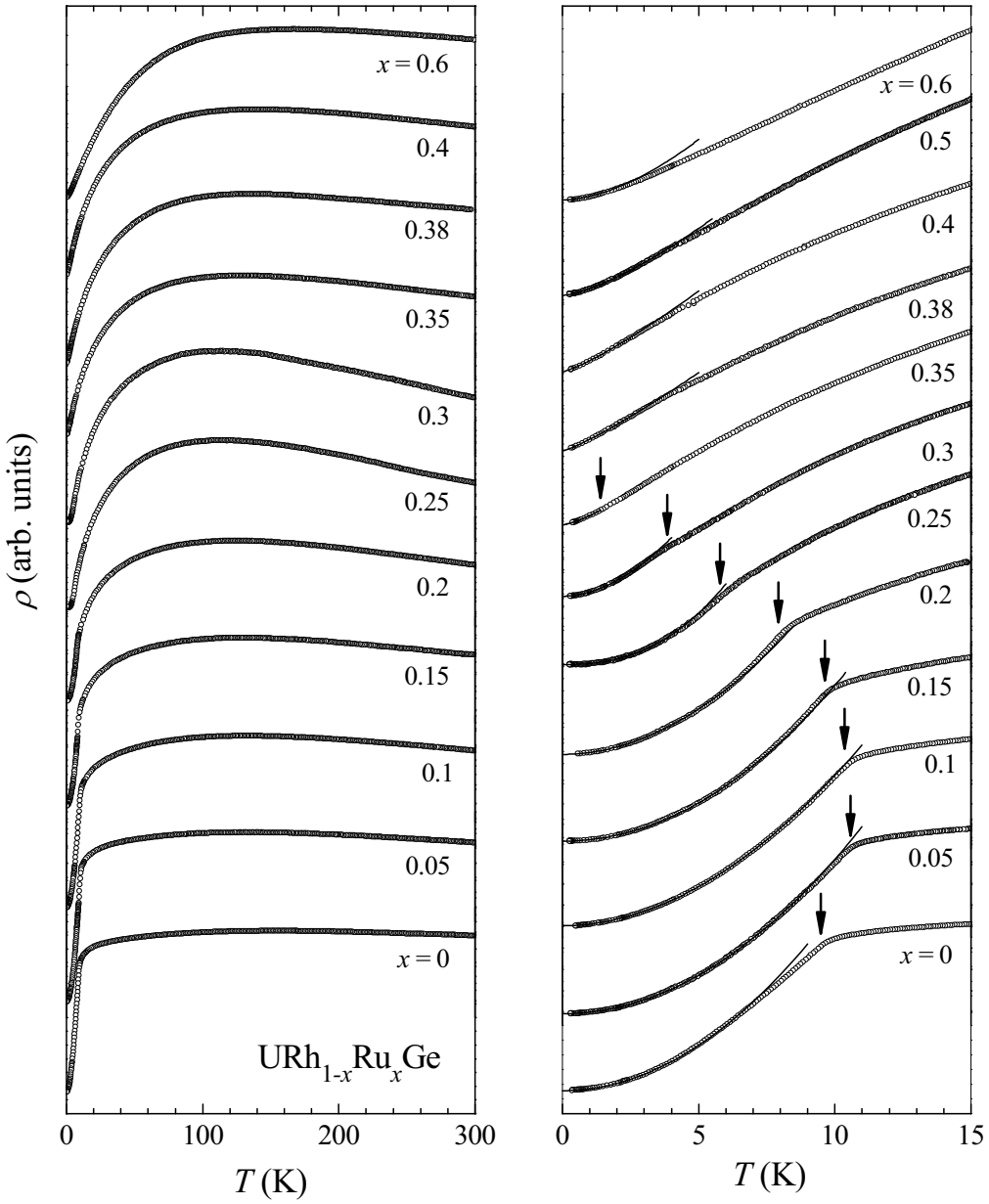

Figure 4.11 Temperature dependence of the electrical resistivity ρ in arbitrary units of $URh_{1-x}Ru_xGe$ alloys for $0 \leq x \leq 0.6$ as indicated. *Left panel*: 2 K $\leq T \leq$ 300 K. *Right panel*: 0.25 K $\leq T \leq$ 15 K. The Curie temperatures are indicated by arrows. The solid lines are fits to Eq. 4.5.

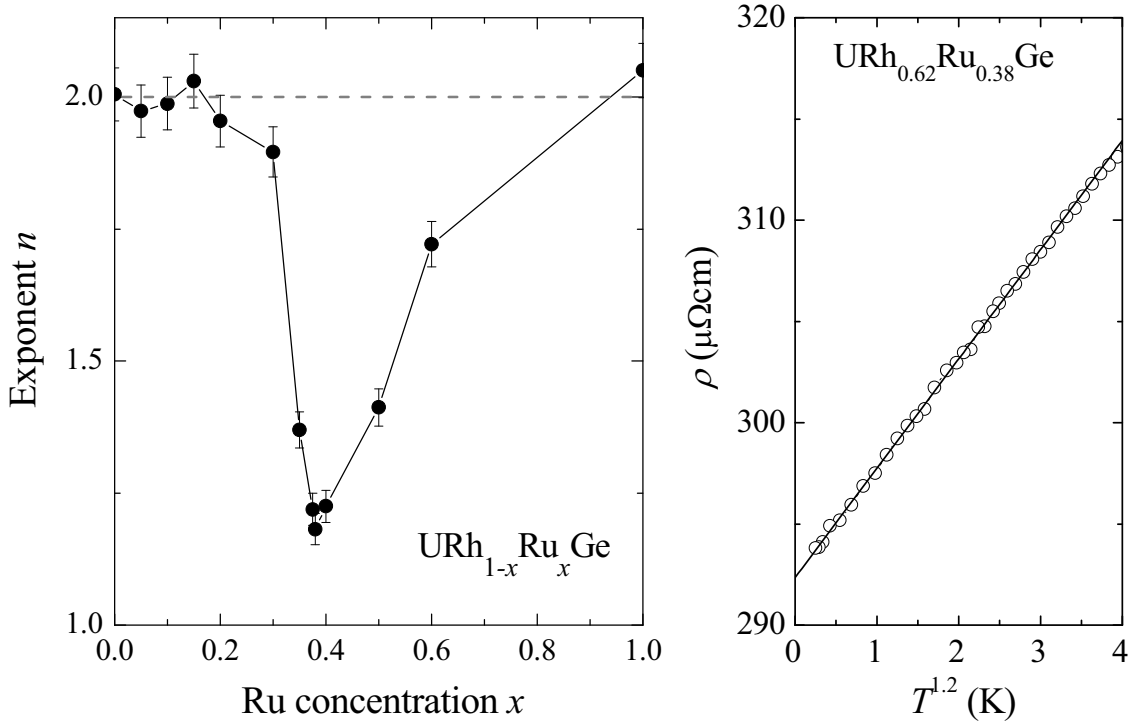

Figure 4.12 Left panel: The exponent n of the $\rho \sim T^{n}$ term in the electrical resistivity of $URh_{1-x}Ru_xGe$ alloys versus Ru concentration. The horizontal dashed line indicates $n = 2$. *Right panel*: The resistivity of $URh_{0.62}Ru_{0.38}Ge$ versus $T^{1.2}$. The solid line represents a fit of the data to $\rho \sim T^{1.2}$.

identified by the maximum in dρ/dT (arrows in Fig. 4.11). The Curie temperatures determined in this way (see Table 4.2) are in good agreement with those obtained by magnetization measurements.

For a ferromagnet with gapped magnon modes, the resistivity in the temperature range below T_C can be well described by Eq. 4.4 [133]:

$$\rho = \rho_0 + AT^n + BT(1 + 2k_BT/\Delta)e^{-\Delta/k_BT} \qquad (4.4)$$

The second term is the electron-electron scattering term (*i.e.* the FL term when $n = 2$) and the third term is due to scattering from magnons. For $0.05 \leq x \leq 0.20$, fits reveal that the second term is dominant $A \gg B$ and $\rho(T) \sim T^{2.0\pm0.1}$ over a wide T range in the ferromagnetic state (see Fig. 4.11). Therefore scattering from magnons can be neglected in the polycrystalline samples of $URh_{1-x}Ru_xGe$ and we restrict the analysis to fitting by:

$$\rho = \rho_0 + AT^n \qquad (4.5)$$

The values of n extracted (by taking the best fit over the largest T interval) are shown in the left panel in Fig. 4.12. $n(x)$ attains a minimum NFL value $n \simeq 1.2$ at a critical concentration

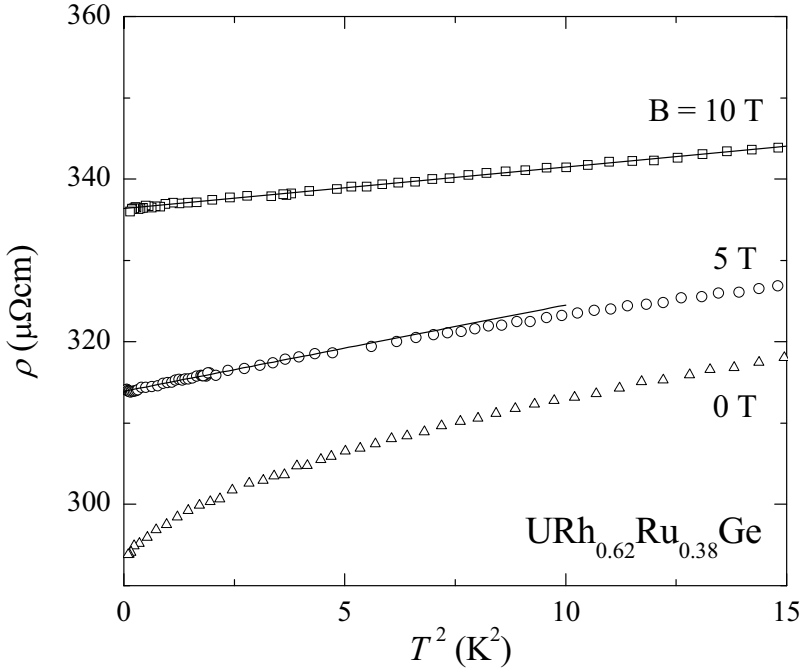

Figure 4.13 The resistivity of $URh_{0.62}Ru_{0.38}Ge$ at different magnetic fields plotted versus T^2. The fields (oriented perpendicular to the current) are (from bottom to top) B = 0, 5 and 10 T. The lines represent fits of the data to $\rho \sim T^2$.

Table 4.2 The Curie temperature and the parameters ρ_0, n and A obtained by fitting the resistivity to $\rho = \rho_0 + AT^n$ (Eq. 4.5) for $URh_{1-x}Ru_xGe$ alloys.

x-Ru	T_C (K)	ρ_0 (μΩcm)	n	A (μΩcm/K^n)
0	9.4	78	2	6.21
0.05	10.5	247	2	3.54
0.1	10.3	300	2	2.14
0.15	9.6	297	2	1.27
0.2	7.9	238	1.95	1.59
0.3	3.8	476	1.89	3.28
0.35	1.3	417	1.37	6.75
0.375	-	385	1.22	6.69
0.38	-	294	1.18	5.40
0.4	-	483	1.23	7.94
0.5	-	247	1.41	5.36
0.6	-	475	1.72	1.66
1	-	132	2.05	0.03

x_{cr} = 0.38 (see the right panel of Fig. 4.12), followed by a slow recovery to the FL value n = 2 there above. The fit parameters are collected in Table 4.2. The resistivity of the compound with x_{cr} = 0.38 is measured in several magnetic fields as shown in Fig. 4.13. In magnetic field of 5 and 10 T a T^2 behavior is observed up to 2 and 4 K, respectively. This demonstrates that the FL state is recovered in a magnetic field.

4.5. Specific heat

The specific heat, c, of the $URh_{1-x}Ru_xGe$ series is measured in zero magnetic field in the temperature interval 0.5 - 20 K. In Fig. 4.14, we show the specific heat divided by temperature c/T of selected $URh_{1-x}Ru_xGe$ alloys with $x \leq 0.3$. In this temperature range both the lattice c_{lat} and the magnetic (*i.e. f*-electron) c_{mag} term contribute to the specific heat: $c = c_{lat} + c_{mag}$. For all samples the lattice contribution is estimated by $c_{lat} = \beta T^3$, by fitting the data in the temperature range $T_C < T < 20$ K, with $\beta = 0.60\times10^{-3}$ J/molK^4. The Debye temperature θ_D = 210 K is calculated through the relation:

$$\theta_D^3 = 3\times\frac{12\pi^4 R}{5\beta} \qquad (4.6)$$

and agrees well with the value reported in Ref.[119]. Here R = 8.314 JK^{-1}mol^{-1} is the gas constant.

For x = 0, the magnetic specific heat for $T \leq 5$ K is described by:

$$c_{mag} = \gamma T + \delta T^{3/2} \qquad (4.7)$$

where γ is the linear coefficient of the electronic specific heat and the second term corresponds to the ferromagnetic spin-wave contribution [134]. The values for γ = 0.150 J/molK^2 and δ = 0.024 J/molK$^{5/2}$ extracted by fitting the data are in good agreement with the values reported in Ref.[119].

In the ordered state the c/T behavior at low temperature dramatically changes upon doping, even for small amounts of Ru concentration (see for instance the data for x = 0.05 in Fig. 4.14). This we attribute to the opening of an energy gap Δ in the magnon spectrum [134] and the magnetic specific heat then follows the relation:

$$c_{mag} = \gamma T + \delta T^{3/2} e^{-\Delta/k_B T} \qquad (4.8)$$

Fits using Eq. 4.8 to the c/T data yield parameters γ = 0.146 and 0.136 J/molK^2, δ = 0.041

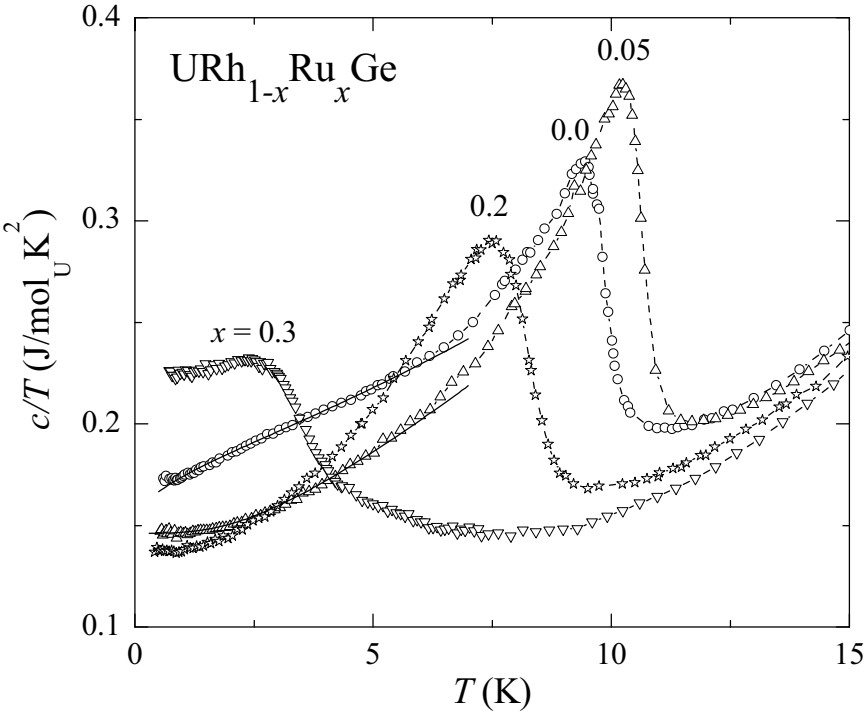

Figure 4.14 Low-temperature specific heat in a plot of c/T versus T of selected $URh_{1-x}Ru_xGe$ alloys with $x \leq 0.3$. The solid lines represent fits to Eq. 4.7 and Eq. 4.8 (with addition of the lattice contribution) for $x = 0$ and $x = 0.05$, respectively.

and 0.094 J/molK$^{5/2}$, and Δ/k_B = 6.5 and 10.6 K for x = 0.05 and 0.1, respectively. (The data for x = 0.1 are not shown in Fig. 4.14).

The FM transition results in pronounced anomalies and the Curie temperature is identified by the inflection points in c/T at the high T side of the peaks. The variation of T_C with x obtained from c/T is consistent with magnetization and transport data. Upon doping, T_C initially increases, but for $x > 0.05$ the ordering peak shifts toward lower T and the transition becomes broader.

In Fig. 4.15, we plot the *f*-electron specific heat divided by temperature, c_{mag}/T, obtained after subtracting the lattice contribution, on a logarithmic temperature scale for $0 \leq x \leq 0.5$. The magnetic transition progressively moves to lower temperature, becomes weaker with increasing x (notably for x = 0.35) and is pushed to below 0.5 K for x = 0.38. This is the characteristic behavior of a metallic-magnet close to a quantum critical point, as observed in many doping-induced NFL systems [10,27,135,136]. For the critical concentration x_{cr} = 0.38, c_{mag}/T presents the NFL behavior as expressed in Eq. 4.9 over one and half decade intemperature, *i.e.* T between 0.5 and 9 K, with b = 0.062 J/molK^2 and the scaling temperature T_0 = 41 K. Beyond x_{cr}, c_{mag}/T deviates from the ln$T$ behavior and tends to

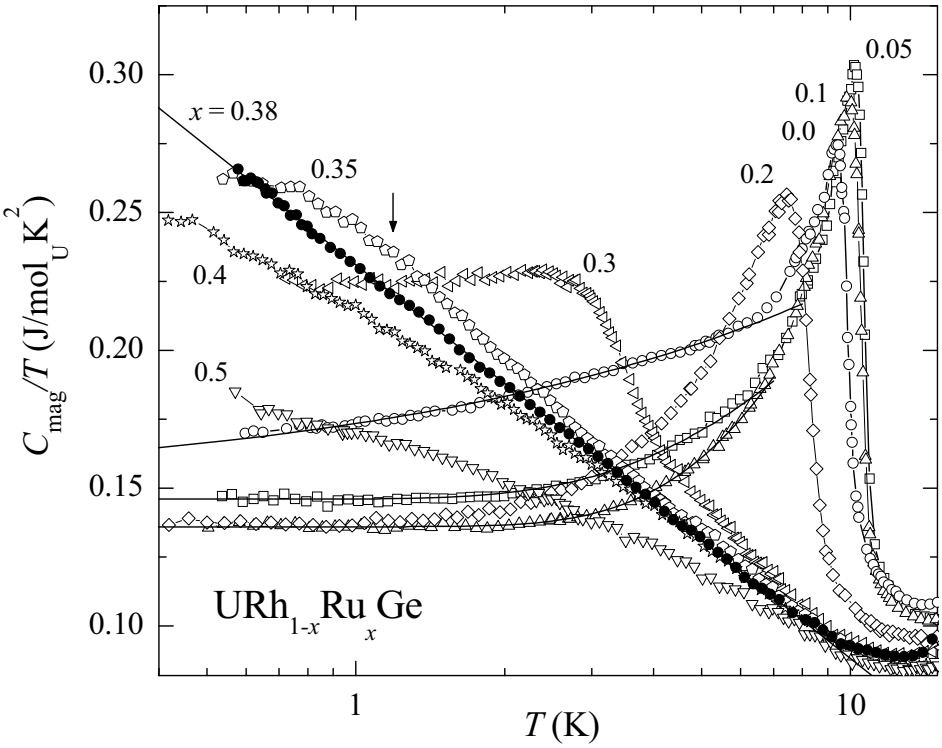

Figure 4.15 f-electronic specific heat of $URh_{1-x}Ru_xGe$ with $0 \le x \le 0.5$ plotted as c_{mag}/T versus T (on a logarithmic scale). The arrow indicates T_C for $x = 0.35$. For $x_{cr} = 0.38$ (•), the straight solid line represents $c_{mag}/T \sim \ln T$ over one and half decade in T. The solid lines represent fits to Eq. 4.7 for $x = 0$, Eq. 4.8 for $x = 0.05$ and 0.1, and Eq. 4.9 for $x = 0.38$.

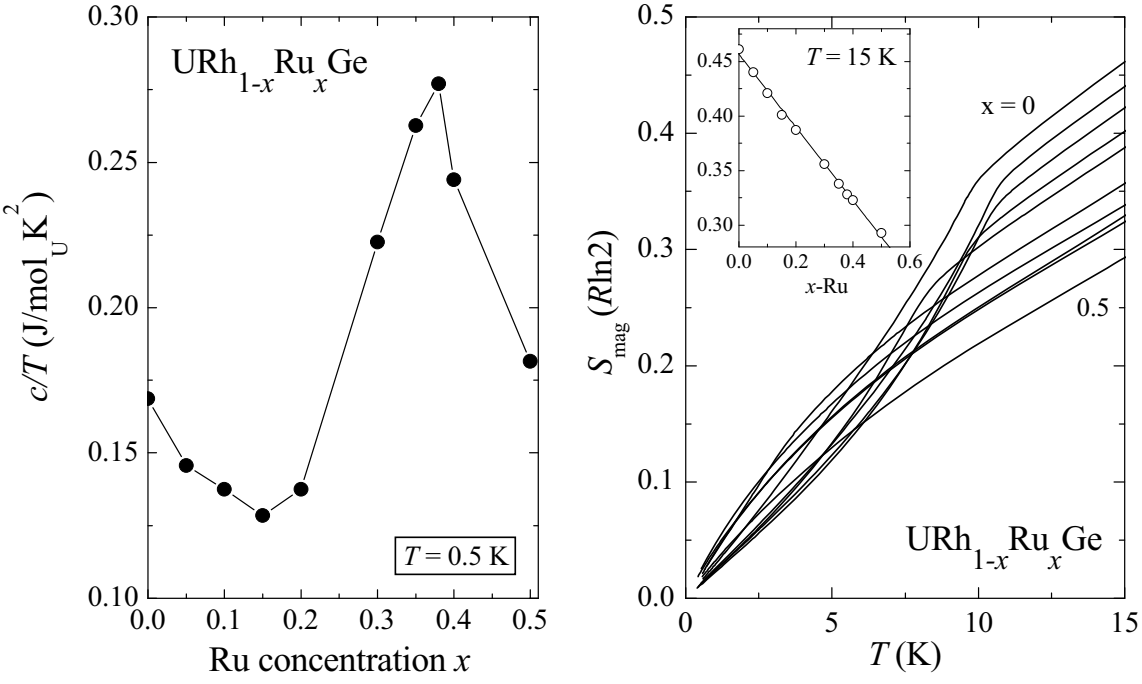

Figure 4.16 Left panel: The γ value at 0.5 K as a function of Ru concentration. *Right panel*: The magnetic entropy S_{mag} (in units of Rln2) for $URh_{1-x}Ru_xGe$ alloys with $0 \le x \le 0.5$. *Inset*: Concentration dependence of S_{mag} at a fixed temperature of 15 K.

saturate at low temperature. This implies FL behavior $c/T \sim \gamma$ is recovered at low temperature.

$$c_{mag} / T = -b \ln \frac{T}{T_0} \qquad (4.9)$$

Table 4.3 The Curie temperature, c/T at 0.5 K and S_{mag} at 15 K of $URh_{1-x}Ru_xGe$ alloys extracted from the specific heat data.

x-Ru	T_C (K)	$c/T_{0.5K}$ (J/molK^2)	$S_{mag,15K}$ (Rln2)
0	9.5	0.169	0.46
0.05	10.4	0.146	0.44
0.1	10.3	0.138	0.42
0.15	9.6	0.129	0.40
0.2	7.8	0.138	0.39
0.3	3.5	0.223	0.36
0.35	1.2	0.262	0.34
0.38	-	0.277	0.33
0.4	-	0.244	0.32
0.5	-	0.181	0.29

The concentration dependence of the γ coefficient is estimated by the c/T value at 0.5 K. A pronounced maximum of c/T at 0.5 K is obtained at x_{cr} (see the left panel of Fig. 4.16).

The spin and charge degrees of freedom of the *f*-electrons contribute to the magnetic entropy S_{mag}, which is calculated by integrating c_{mag}/T versus T between 0.5 and 15 K and shown in the right panel of Fig. 4.16. For $x = 0$, S_{mag} is about 50% compared to the ideal value, Rln2, of a magnetic system with localized moments ($S = ½$). This confirms the itinerant nature of the FM transition. The linear decrease of S_{mag} with x shows the system becomes more itinerant upon Ru doping.

4.6. ac-susceptibility

Upon approaching the magnetic instability, the ferromagnetic transition becomes less pronounced in the transport and specific heat data, while the dc-magnetization has been measured down to 2 K only. Therefore, we carried out ac-susceptibility measurements at low temperatures ($T \geq 0.25$ K) for a few samples close to x_{cr}.

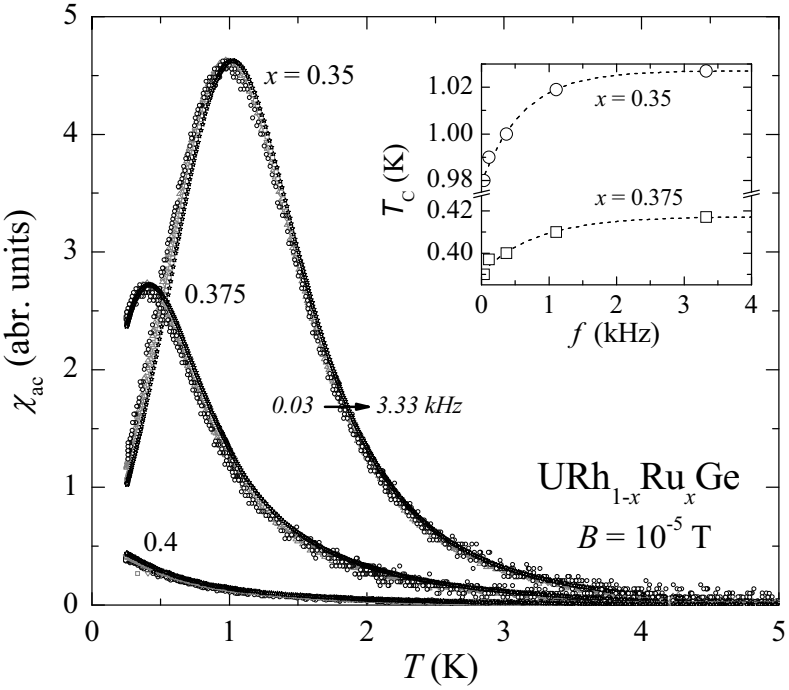

Figure 4.17 Temperature dependence of the ac-susceptibility in $URh_{1-x}Ru_xGe$ for x = 0.35, 0.375 and 0.4 at frequencies f = 0.03, 0.11, 0.35, 1.11 and 3.33 kHz. The data are scaled to the maximum amplitude of χ_{ac} at 3.33 kHz using multiplication factors of 1 ± 0.03 for f = 0.11, 0.35 and 1.11 kHz and ~ 1.2 for f = 0.03 kHz. The inset shows $T_C(f)$.

Fig. 4.17 shows the ac-susceptibility results, χ_{ac}, measured in a driving field of 10^{-5} T for x = 0.35 and 0.375. The maxima in χ_{ac} signal FM order. For x = 0.35, the ordering peak is located at T_C = 1.0 K. This value is somewhat smaller than the values deduced from the Arrott plot (1.3 K) and from the specific heat (1.2 K). On the other hand T_C = 0.4 K for x = 0.375 nicely falls on the straight line with dT_C/dx = -0.43 K/at.%Ru (see Section 4.7.1), as expected. For x = 0.4, no magnetic ordering is detected, χ_{ac} weakly increases with decreasing temperature down to 0.25 K. These χ_{ac} data are in line with the notion of magnetism vanishing at x_{cr} = 0.38. The frequency dependence of χ_{ac}, investigated in the range 0.03 - 3.33 kHz, is weak, as follows from the near overlap of the curves in Fig. 4.17. $T_C(f)$ shows a small initial increase, but then saturates with $\Delta T_C/T_C \sim 5\%$ near the maximum frequency. The amplitude of χ_{ac} initially increases but is virtually constant for $f \geq 0.11$ kHz, (see caption of Fig. 4.17).

The χ_{ac} results manifestly differ from those recently reported for x = 0.30 [137] where a strong frequency dependence of χ_{ac} was taken as evidence for short-range rather than long-range magnetic order. The difference was also observed in dc-magnetization results.

Whereas in Ref.[137] no spontaneous magnetization was detected for x = 0.30, proper Arrott plots are derived at least up to x = 0.325 in this work (see Fig. 4.5). These dissimilar results are attributed to a different sample quality, which may vary with the preparation method and annealing procedure.

4.7. Discussion

4.7.1. The magnetic phase diagram

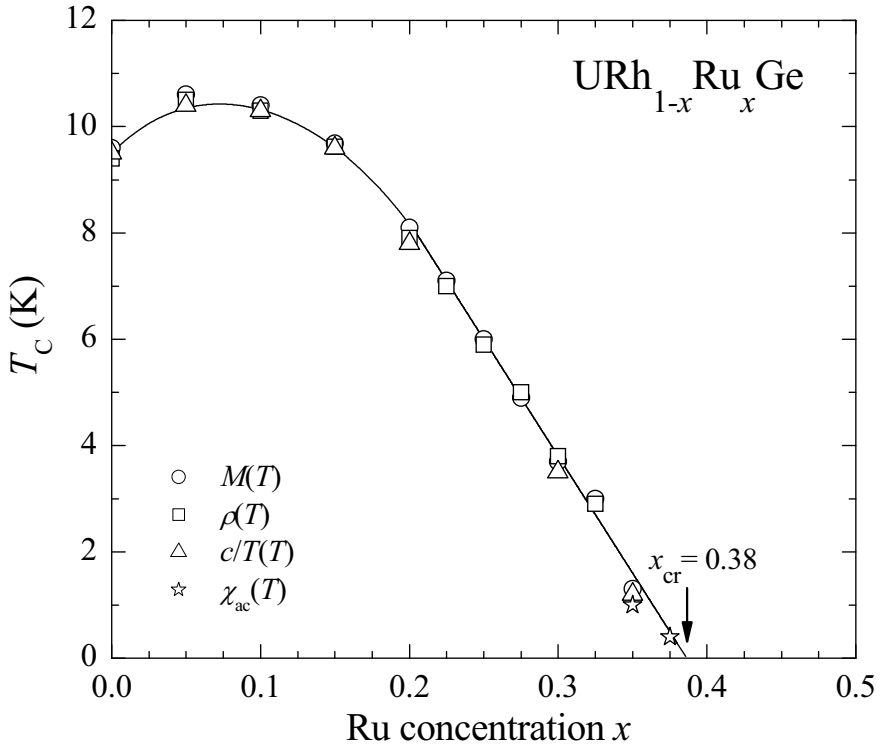

Figure 4.18 The Curie temperature of $URh_{1-x}Ru_xGe$ alloys as a function of Ru concentration determined from $M(T)$, $\rho(T)$, $c(T)$ and $\chi_{ac}(T)$. T_C is suppressed with a rate of -0.43 K/at.%Ru from x = 0.2 onwards (The data magnetization point for x = 0.35 is obtained by extrapolation in the Arrott plot). The line serves to guide the eye.

By tracing the $T_C(x)$ values determined from magnetization, resistivity, specific heat and ac-susceptibility experiments we can construct the magnetic phase diagram of URhGe doped with Ru (see Fig. 4.18). The Curie temperatures obtained by the different experiments are equal within the experimental error. T_C first increases, has a maximum near x = 0.05 then linearly decreases at a rate of -0.43 K/at.% Ru and vanishes near the critical concentration x_{cr} = 0.38.

A parallel study on $URh_{1-x}Ru_xGe$ alloys has been reported in Ref.[138]. These authors

report that ferromagnetic order vanishes at x = 0.25, where the system undergoes a crossover into a nonmagnetic ground state with short-range magnetic interactions for x between 0.3 and 0.35. We attribute these the dissimilar results to a different sample quality. Moreover the measurements in Ref.[138] have been carried out in the temperature range above 2 K only, which hampers a proper analysis of the critical phenomena.

4.7.2. Hybridization phenomena

The evolution of magnetic order in correlated 4*f*- and 5*f*-electron metals is often discussed in terms of a simple Doniach picture [28], where the competition between the on-site Kondo interaction and inter-site RKKY (Ruderman-Kittel-Kasuya-Yosida) interaction determines the ground state. In the Doniach model the control parameter is the ratio of the exchange interaction J over the bandwidth W. Keeping W constant, a weak hybridization (J small) favours the RKKY interaction and a magnetic ground state, while a strong hybridization (J large) favours a non-magnetic Kondo-screened ground state. In the generic Doniach phase diagram the magnetic ordering temperature T_M goes through a maximum with increasing J and vanishes when the RKKY and Kondo energies become comparable (see Fig. 3.1). A typical example of a ferromagnetic material that follows the generic Doniach phase diagram is cubic CeAg (T_C = 5.6 K) [139]. Here hydrostatic pressure is used to control J via the unit cell volume, such that $T_C(p)$ goes through a broad maximum near 0.7 GPa. For the orthorhombic U*TX* alloys (*X* is Ge or Si) the effect of chemical substitutions does not scale with the unit cell volume but critically depends on the relative change in the lattice parameters. Resistivity measurements under hydrostatic pressure on pure URhGe show that T_C increases linearly up to very high pressures (T_C reaches ≈ 17 K at 13 GPa) [120].

Nevertheless, it is interesting to compare the volume effects due to alloying and hydrostatic pressure. Assuming an isothermal compressibility $\kappa = -V^{-1}(dV/dp)$ of about 0.8 Mbar^{-1} [121], substitution of 1 at.% Ru leads to a chemical pressure of 0.37 kbar. Using dT_C/dp = 0.065 K/kbar as derived from the resistivity measurements under pressure [120] an increase of T_C of 0.024 K per at.% Ru is calculated. In the case of Ru doping, these calculated values are about a factor 5 too small when compared to the measured initial increase in T_C. Clearly, chemical and mechanical pressures give different results. Magnetization measurements under pressure on URhGe doped with 32.5 at.% Ru (T_C = 2.8 K at ambient pressure) did not show a noticeable change of T_C for a pressure of 4.3 kbar [140]. This indicates an additional complication, namely dT_C/dp varies with

doping concentration.

In a simple model, extracting electrons from the *d*-band results in an additional strengthening of the *f-d* hybridization, which in turn leads to a larger exchange parameter *J*, favoring the Kondo interaction. This idea is supported by the specific-heat measurement. The linear coefficient of the electronic specific heat γ increases as a function of x and reaches a maximum value near the critical concentration (see the left panel in Fig. 4.16). The 5*f*-4*d* hybridization mechanism was also used to explain the suppression of ferromagnetic order in the analogous compounds URhAl and URhGa doped with Ru [141]. It would be interesting to investigate whether more sophisticated models, like the one proposed by Sheng and Cooper [142], could explain the observed behaviour of the magnetic ordering temperature. By incorporating the change in the *f*-density spectral distribution under pressure in the linearized muffin-tin orbitals (LMTO) band-structure calculations, these authors could explain the observed maximum in the magnetic ordering temperature for compounds like UTe. More recently, theoretical results were presented for the underscreened Kondo-lattice model with localized $S = 1$ spins coupled to a conduction band through a Kondo coupling J_K and interacting among them ferromagnetically [143]. For large values of J_K the Kondo effect is found to coexist with ferromagnetic order with $T_K > T_C$. However, the proposed ferromagnetic Doniach-like diagram does not exhibit a critical point for ferromagnetism.

The valence bands of $URh_{1-x}Ru_xGe$ ($x \leq 0.4$) have been investigated by X-ray photoemission at room temperature [144]. A relatively weak modification of the valence band structure is observed for $x \leq 0.3$. The spectra show a similar structure of the density of states (DOS) near the Fermi level. The spectra are dominated by two peaks at 2.7 and 0.7 eV. The latter peak is narrow (~ 1 eV) and can be attributed to the 5*f* states. The structure at 2.7 eV represents the superimposed Rh and Ru states, which form a broad band (~ 4 eV). Interestingly, a rapid change occurs for $0.35 \leq x \leq 0.4$: the 4*d* peak position shift to lower binding energy and the 5*f* structure becomes less resolved. The sudden evolution of the DOS in this concentration range coincides with the loss of magnetism near the critical concentration $x = 0.38$. It would be highly interesting to investigate and resolve the valence band structure at liquid helium temperatures.

4.7.3. Ferromagnetic quantum critical point

The $c(T)$, $\rho(T)$, $M(T)$ and $\chi_{ac}(T)$ data of the $URh_{1-x}Ru_xGe$ alloys provide evidence for a

continuous FM quantum phase transition at $x_{cr} = 0.38$.

The most compelling evidence is the specific heat $c/T \sim \ln(T/T_0)$ observed over one and a half decade in T (see Fig. 4.15) and the concomitant maximum in $c/T_{0.5K}(x)$ (see the left panel in Fig. 4.16). The temperature $T_0 = 41$ K is large, which indicates that our $c(T)$ experiments down to $T = 0.4$ K ($T/T_0 \approx 0.01$) indeed probe the quantum critical regime. It will be interesting to investigate whether the $c/T \sim \ln T$ behavior persists even at lower T. Eventually, however, c/T will saturate because of crystallographic disorder inherent to the $URh_{1-x}Ru_xGe$ alloys.

Further support for a QCP is provided by the critical behavior in the resistivity $\rho_{cr} \sim T^{1.2}$ up to 2 K. The exponent $n(x)$ has a pronounced minimum at x_{cr} (see the left panel in Fig. 4.12). The value $n \simeq 1.2$ is smaller than the value $n = 5/3$ predicted for a clean FM QCP [82]. This is not unexpected as disorder reduces n [85]. However, we stress the sharp minimum near x_{cr} with $n \simeq 1.2$ is an intrinsic feature of the FM QCP. The value $n = 2$ is recovered for $x > 0.38$. For $x_{cr} = 0.38$, the $\rho \sim T^2$ temperature dependence is recovered under applied magnetic field and T_{FL}, the temperature where the T^2-fit deviates from the measurements increases with the field (see Fig. 4.13). This indicates that the magnetic field tunes the system away from the critical point and that the FL state is recovered.

The itinerant nature of the FM state and the smooth suppression of M_S pointing to a continuous phase transition strongly suggest that the QPT in $URh_{1-x}Ru_xGe$ is of the Hertz-Millis type [80,81], albeit with modified exponents due to the effects of doping (notably emptying the *d* band and alloy disorder). For instance, for an itinerant clean FM QPT, one expects $T_C \sim (x_{cr} - x)^{3/4}$ (dimension $d = 3$, dynamical critical exponent $z = 3$), while $T_C \sim (x_{cr} - x)$ is obtained over a wide range $0.20 \leq x \leq 0.375$. Deviations from the clean behavior are also observed in *f*-electron materials with pressure- and doping-induced continuous FM QPT, such as $CeSi_{1.81}$ [16] and $CePd_{1-x}Rh_x$ [27], respectively. On the other hand, for *d*-electron alloys with a continuous FM QPT (*e.g.*, Ni_xPd_{1-x} [23] and $Zr_{1-x}Nb_xZn_2$ [25]), the data are to a large extent in agreement with the itinerant model. Further theoretical work is required to clarify these issues.

In conclusion, the suppression of ferromagnetism in the $URh_{1-x}Ru_xGe$ series is investigated. The thermal, transport, and magnetic data provide evidence for a continuous FM quantum phase transition at the critical concentration $x_{cr} = 0.38$. The $URh_{1-x}Ru_xGe$ alloys are unique in the sense that they present the first *f*-electron system with a FM QCP at ambient pressure (notice the vanishing of FM order in $CePd_{1-x}Rh_x$ is very much “smeared” [27]).